

The composition of a disrupted extrasolar planetesimal at SDSS J0845+2257 (Ton 345)

D. J. Wilson,¹★ B. T. Gänsicke,¹ D. Koester,² O. Toloza,¹ A. F. Pala,¹ E. Breedt¹ and S. G. Parsons³

¹Department of Physics, University of Warwick, Coventry CV4 7AL, UK

²Institut für Theoretische Physik und Astrophysik, University of Kiel, D-24098 Kiel, Germany

³Departamento de Física y Astronomía, Universidad de Valparaíso, Avenida Gran Bretaña 1111, Valparaíso 2360102, Chile

Accepted 2015 May 22. Received 2015 May 22; in original form 2015 February 20

ABSTRACT

We present a detailed study of the metal-polluted DB white dwarf SDSS J0845+2257 (Ton 345). Using high-resolution *Hubble Space Telescope*/Cosmic Origins Spectrograph and Very Large Telescope spectroscopy, we have detected hydrogen and 11 metals in the atmosphere of the white dwarf. The origin of these metals is almost certainly the circumstellar disc of dusty and gaseous debris from a tidally disrupted planetesimal, accreting at a rate of $1.6 \times 10^{10} \text{ g s}^{-1}$. Studying the chemical abundances of the accreted material demonstrates that the planetesimal had a composition similar to the Earth, dominated by rocky silicates and metallic iron, with a low water content. The mass of metals within the convection zone of the white dwarf corresponds to an asteroid of at least $\sim 130\text{--}170$ km in diameter, although the presence of ongoing accretion from the debris disc implies that the planetesimal was probably larger than this. While a previous abundance study of the accreted material has shown an anomalously high mass fraction of carbon (15 per cent) compared to the bulk Earth, our independent analysis results in a carbon abundance of just 2.5 per cent. Enhanced abundances of core material (Fe, Ni) suggest that the accreted object may have lost a portion of its mantle, possibly due to stellar wind stripping in the asymptotic giant branch. Time series spectroscopy reveals variable emission from the orbiting gaseous disc, demonstrating that the evolved planetary system at SDSS J0845+2257 is dynamically active.

Key words: planets and satellites: composition – stars: individual: SDSS J0845+2257 – planetary systems – white dwarfs.

1 INTRODUCTION

Since the discovery of calcium absorption lines in the atmosphere of van Maanen 2 (van Maanen 1917; Weidemann 1960), an explanation has been sought for the metal pollution observed in many white dwarfs. The high surface gravity ($\log g$) of white dwarfs implies that all metals will sink out of their atmospheres on time-scales that are short relative to the cooling age, leaving pristine hydrogen or helium atmospheres. However, metal pollution is now thought to be present at 25–50 per cent of all white dwarfs (Zuckerman et al. 2003, 2010; Barstow et al. 2014; Koester, Gänsicke & Farihi 2014a). Whilst radiative levitation can explain the observed metals in some white dwarfs with effective temperatures (T_{eff}) above 20 000 K (Chayer, Fontaine & Wesemael 1995; Chayer 2014; Koester et al. 2014a), metal-polluted white dwarfs cooler than this must be currently ac-

creted, or have recently accreted, material from an external source (Koester 2009).

Historically the source of this accretion was thought to be the interstellar medium (Aannestad & Sion 1985; Sion, Aannestad & Kenyon 1988). The explanation that is now generally accepted developed from the infrared detection of a dusty debris disc, formed by the tidal disruption of an asteroid, around the white dwarf G29-38 (Zuckerman & Becklin 1987; Graham et al. 1990; Jura 2003). Since then more than 30 similar discs have been discovered, and current estimates suggest that 1–3 per cent of white dwarfs possess detectable dusty debris discs (Farihi, Jura & Zuckerman 2009; Girven et al. 2011; Steele et al. 2011; Barber et al. 2014; Rocchetto et al. 2015). Debris from these disrupted planetesimals accreting on the white dwarfs is now thought to be the dominant source of the atmospheric metals. In summary, these discoveries reveal the presence of evolved planetary systems at white dwarfs, offering an insight into the end stages of planetary evolution. Zuckerman (2015) noted that, in hindsight, the discovery of van Maanen 2 was

* E-mail: d.j.wilson.1@warwick.ac.uk

Table 1. Log of observations of SDSS J0845+2257.

Date	Telescope/ instrument	Wavelength range (Å)	Spectral resolution (Å)	Total exposure time (s)
2004 December 19	SDSS	3794–9199	0.9–2.1	3300
2008 January 02	WHT/ISIS	3577–8840	1.0–2.0	2400
2008 April 03–5	VLT/UVES	3280–9460	0.02	17 820
2008 January 08	VLT/UVES	3280–9460	0.02	11 880
2009 April 09–11	VLT/UVES	3280–9460	0.02	17 820
2010 March 31	<i>HST</i> /COS	2470–3150	0.01	7727
2010 April 01	<i>HST</i> /COS	1600–3150	0.39	14 397
2010 April 02	Gemini South/GMOS	7540–9665	2.0	4980
2011 January 29	VLT/X-shooter	2990–24 790	0.2–0.6	6990
2014 October 20	VLT/X-shooter	2990–24 790	0.2–0.6	3731

therefore the first observational evidence of an extrasolar planetary system.

In most white dwarfs, pollution from only one or two elements, usually Ca and/or Mg, has been detected. However, high-resolution spectroscopy of an increasing number of systems has revealed pollution by large number of metals, with a record of 16 species detected in the case of GD 362 (Xu et al. 2013). Around a dozen white dwarfs show photospheric O, Mg, Si and Fe (Klein et al. 2011; Dufour et al. 2012; Gänsicke et al. 2012; Jura et al. 2012; Farihi, Gänsicke & Koester 2013; Xu et al. 2014; Raddi et al. 2015). These four elements make up >90 per cent of the bulk Earth (Allège, Manhès & Lewin 2001).

Consequently, these systems provide a unique opportunity to study the bulk chemical composition of extrasolar planetary systems. Thus far, two main conclusions have been reached. (1) To zeroth order the chemical composition of the accreted debris is similar to that of the terrestrial planets in the Solar system (Zuckerman et al. 2007; Jura & Young 2014), with a distinct lack of volatile elements (Jura 2006; Farihi et al. 2009). (2) Within this overall similarity, there is a large amount of diversity, with some systems showing evidence of differentiation (Gänsicke et al. 2012), post-nebula processing (Xu et al. 2013) and water-rich asteroids (Farihi et al. 2013; Raddi et al. 2015).

We present ultraviolet and time series optical spectra of the metal-polluted DB white dwarf SDSS J084539.17+225728.0 (henceforth SDSS J0845+2257). This object was originally classified as a sdO subdwarf, Ton 345 (Green, Schmidt & Liebert 1986). As part of a search for Ca II 8600 Å emission lines among white dwarfs with SDSS spectra, Gänsicke et al. (2008) found that SDSS J0845+2257 was in fact a DB (helium atmosphere) white dwarf with a gaseous disc. Follow-up observations obtained with the William Herschel Telescope (WHT) revealed a significant change in the shape and strength of the Ca II 8600 Å emission line profile, along with strong photospheric absorption lines from Ca, Si and Mg.

Jura et al. (2015) presented a Keck/HIRES study detecting 11 metals in the atmosphere of SDSS J0845+2257. We extend these observations into the ultraviolet and carry out an independent detailed study of the accreted material. We also present updated time series observations of variable emission from the gaseous disc around SDSS J0845+2257 and an analysis of the *Hubble Space Telescope* (*HST*)/Cosmic Origins Spectrograph (COS) high-speed ultraviolet photometry.

2 OBSERVATIONS

Since the publication of Gänsicke et al. (2008) we have obtained deep spectroscopic observations of SDSS J0845+2257 in the ultra-

violet with the *HST* and in the optical with the European Southern Observatory (ESO) Very Large Telescope (VLT) and Gemini South. Table 1 provides a log of our observations.

HST observed SDSS J0845+2257 on 2010 March 31 and 2010 April 01 with the COS (Green et al. 2012). Eight orbits were awarded under proposal ID 11561 for a total exposure time of 2735, 4994 and 14397 s with the G130M, G160M and G230L gratings, respectively. The spectra were processed with CALCOS 2.12. Both the FUV (1120–1800 Å, Fig. 1) and NUV (1600–2060 Å, 2470–3150 Å, Fig. 2) spectra show a host of metal absorption lines, with only small amounts of continuum remaining.

Optical observations of SDSS J0845+2257 were obtained at the VLT on 2008 April 03–05, 2009 January 08 and 2009 April 09–11 with the Ultraviolet and Visual Echelle Spectrograph (UVES; Dekker et al. 2000) and again on 2011 January 29 and 2014 October 20 with X-shooter (Vernet et al. 2011). Total exposure times were 47520 s with UVES and 10721 s with X-shooter. These observations were reduced using the standard procedures within the REFLEX¹ reduction tool developed by ESO. A heliocentric correction was applied to the REFLEX outputs, and multiple exposures from the same night were combined (Fig. 3). The optical spectra show a large number of absorption lines, indicative of pollution from a variety of metals. The 8600 Å Ca II emission line triplet is also clearly visible in all of the observations (see Section 5).

On 2010 April 02 we obtained six spectra of SDSS J0845+2257 using the Gemini Multi-object Spectrograph (GMOS) on Gemini South (Hook et al. 2004). The observations were made in service mode, using the R831 grating and a 1 arcsec slit, which gave a wavelength range of 7540–9665 Å at a resolution of 2.0 Å. We requested the acquisition to be done in the *i* band to ensure that the target was properly centred on the slit in the region of the Ca II lines. We reduced and extracted the spectra using the STARLINK software packages KAPPA and PAMELA, and then applied the wavelength and flux calibration using MOLLY.² The wavelength calibration was derived from a CuAr arc exposure taken in the morning following the observations and adjusted according to the known wavelengths of strong night sky emission lines. The flux calibration was calculated using an observation of the spectroscopic standard star LTT 3218. Finally, we combined the six individual exposures to give a single, high-signal-to-noise spectrum with a combined exposure time of

¹The REFLEX software and documentation can be obtained from <http://www.eso.org/sci/software/reflex/>

²MOLLY was written by T. R. Marsh and is available from <http://www.warwick.ac.uk/go/trmarsh/software/>

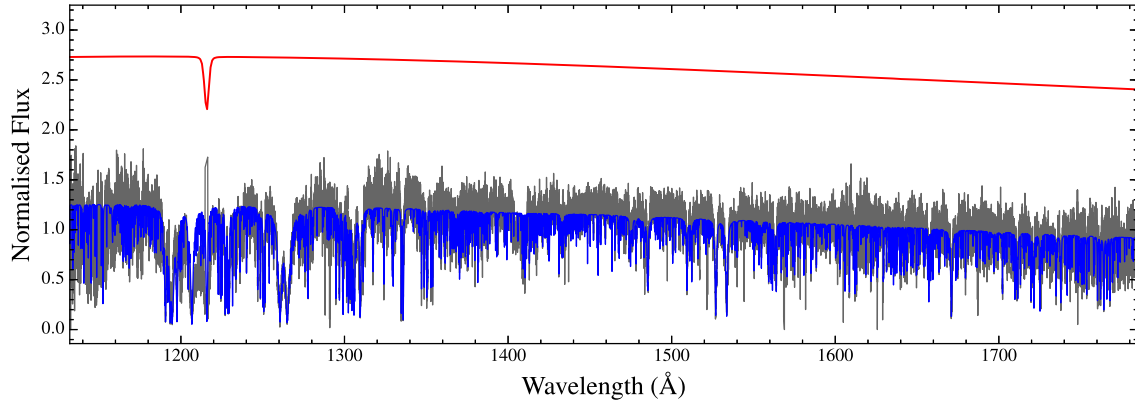


Figure 1. *HST/COS* FUV spectrum of SDSS J0845+2257 obtained on 2010 April 01 (grey), with the model fit used to determine the abundances of the accreted metals (blue). Plotted in red is a model spectrum for a white dwarf with the same atmospheric parameters, but no metals. The extremely large number of metal absorption lines in the spectrum of SDSS J0845+2257 is successfully reproduced by the model fit, with the exception of the two sections shown in Fig. 4.

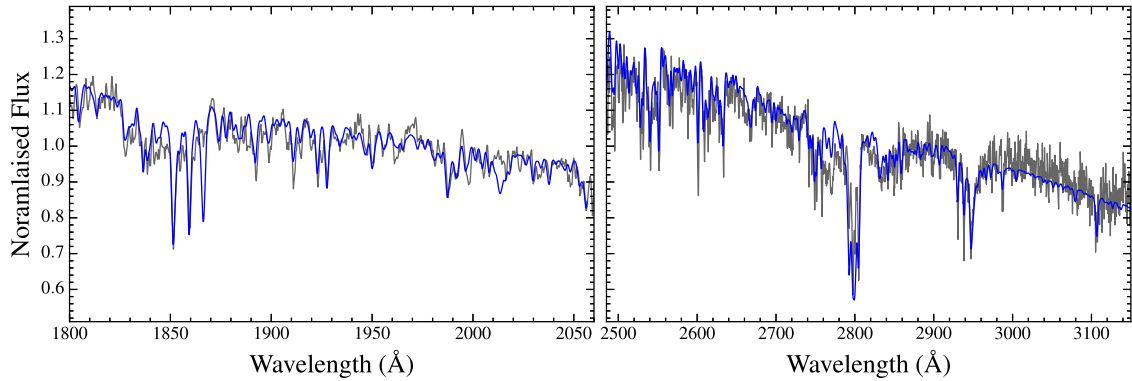


Figure 2. *HST/COS* NUV spectrum of SDSS J0845+2257 obtained on 2010 March 31 (grey), with the model fit used to determine the abundances of the accreted metals (blue). The model underpredicts the Mg II 2790 Å triplet, possibly due to emission from the gaseous debris disc (Section 5).

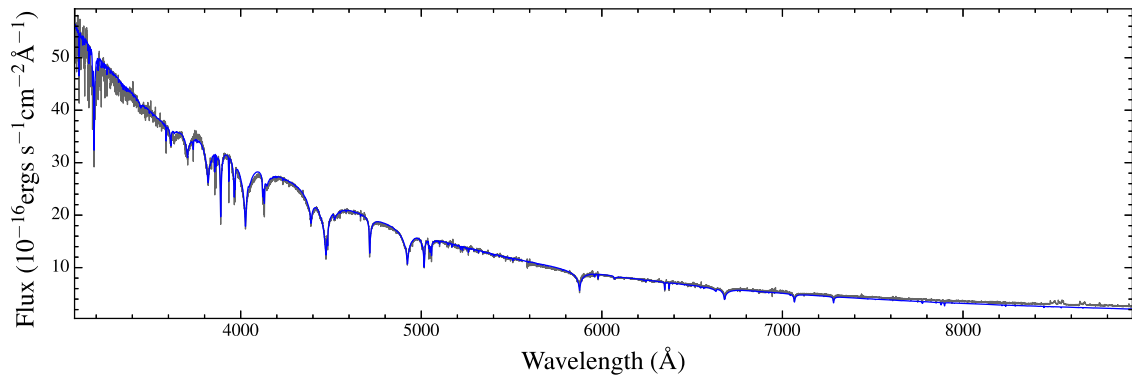


Figure 3. Full optical spectrum of SDSS J0845+2257 from the UVB and VIS arms of X-shooter (grey) together with the model fit (blue) used to calculate the atmospheric parameters and the metal abundances. A telluric correction was applied using the X-shooter spectral library (Chen et al. 2014). The model is overplotted using just one scaling factor for the entire spectrum, demonstrating the excellent flux calibration of the X-shooter data.

4980 s. The strength of the 8600 Å Ca II triplet in this spectrum is comparable to the other optical observations.

3 WHITE DWARF PARAMETERS

The spectroscopic determination of atmospheric parameters for hot DB white dwarfs is extremely difficult, because the spectra hardly change between $T_{\text{eff}} = 20\,000$ and $30\,000$ K. Using a fit

to the SDSS photometry with a fixed $\log g = 8.00$, we obtain $T_{\text{eff}} = 19\,850 \pm 600$ K for a pure He grid, $T_{\text{eff}} = 19\,890 \pm 620$ K for a grid with $\log(\text{H}/\text{He}) = -5.0$ and $T_{\text{eff}} = 19\,880 \pm 600$ K for a grid with our final metal abundances. The increase of the free electron density, which is the major effect from the inclusion of metals in cooler DB models, has no significant effect at these temperatures. There is, however, a noticeable blanketing effect from the strong metal lines in the ultraviolet. This increases the overall flux in the optical range, but with the same factor in all SDSS

band passes. It therefore has no effect on the atmospheric parameter determination.

A possible difficulty when using the photometry for faint and distant objects is the interstellar reddening. The maximum reddening in the direction of SDSS J0845+2257 is $E(B - V) = 0.0268$ (Schlafly & Finkbeiner 2011). If we apply this value and repeat the fitting with the dereddened photometry, the result is a much higher temperature of $T_{\text{eff}} = 24\,320 \pm 920$ K. From the solid angle obtained through this fit, and assuming a radius of the white dwarf which corresponds to $\log g = 8.0$, we can obtain the distance to the white dwarf and estimate the true reddening. We find a distance of 117 pc and a vertical distance above the Galactic plane of 67 pc. Using the algorithm of Tremblay, Bergeron & Gianninas (2011, see also Genest-Beaulieu & Bergeron 2014), we estimate a negligible reddening of $E(B - V) = 0.001$, and thus the lower T_{eff} is secure.

The atmospheric parameters from the photometry are confirmed by a fit to the SDSS spectrum, which results in $T_{\text{eff}} = 19\,800 \pm 70$ K, $\log g = 8.16 \pm 0.02$ for the pure He grid and $T_{\text{eff}} = 19\,780 \pm 70$ K, $\log g = 8.18 \pm 0.02$ for the grid with $\log(\text{H}/\text{He}) = -5.0$. A final test is offered by the absolute calibration of the *HST* spectra. Using the solid angle from the photometry, the effective temperature is confined to $T_{\text{eff}} = 19\,750 \pm 250$ K by the comparison of the predicted ultraviolet fluxes with the observations. Our final compromise for the atmospheric parameters is the spectroscopic fit with the $\log(\text{H}/\text{He}) = -5$ grid, with enlarged errors:

$$T_{\text{eff}} = 19\,780 \pm 250 \text{ K} \quad \log g = 8.18 \pm 0.20.$$

The hydrogen abundance is consistent with a fit to the $\text{H}\alpha$ line found in the UVES spectrum (Fig. 5).

Jura et al. (2015) rely entirely on a fit to the SDSS photometry, obtaining $T_{\text{eff}} = 19\,535 \pm 700$ K for a pure He grid and $T_{\text{eff}} = 18\,700 \pm 700$ K for a grid with the observed metal abundances. The surface gravity cannot be obtained from the photometry so they fixed $\log g = 8.00$. We have computed a model adopting the parameters of Jura et al. (2015) and multiplied it with the solid angle obtained from their photometric fit. Their lower T_{eff} underpredicts the COS ultraviolet fluxes by 15–23 per cent. Whilst a temperature difference of 1000 K would not normally have a large effect on the metal abundances, in this case all elements heavier than oxygen are in a transition from first to second ionization stage so the predicted lines in our, hotter, model are significantly weaker. We thus obtain larger abundances for all elements, with the exception of carbon. Our carbon abundance is based on the COS ultraviolet spectroscopy, which contains more and stronger carbon lines than the optical data analysed by Jura et al. (2015). An independent model atmosphere analysis of the COS ultraviolet spectra of SDSS J0845+2257 carried out by P. Dufour (private communication), adopting our atmospheric parameters, confirms the low photospheric carbon abundance.

Using our results for T_{eff} and $\log g$, and the helium atmosphere models of Bergeron and collaborators,³ we find a cooling age $T_{\text{cool}} \approx 100$ Myr, white dwarf mass $M_{\text{wd}} = 0.679 M_{\odot}$ and radius $R_{\text{wd}} = 0.011 R_{\odot}$. Starting from a Rossland optical depth $\tau_r = 100$ and integrating the envelope equations downwards using the equation of state of Saumon, Chabrier & van Horn (1995), we find a convection zone mass of $\log(M_{\text{cvz}}/M_{\text{wd}}) = -8.4$. Using the initial-to-final mass relationships of Gesicki et al. (2014), Casewell et al.

³ <http://www.astro.umontreal.ca/~bergeron/CoolingModels>, based on Holberg & Bergeron (2006), Kowalski & Saumon (2006), Tremblay et al. (2011) and Bergeron et al. (2011).

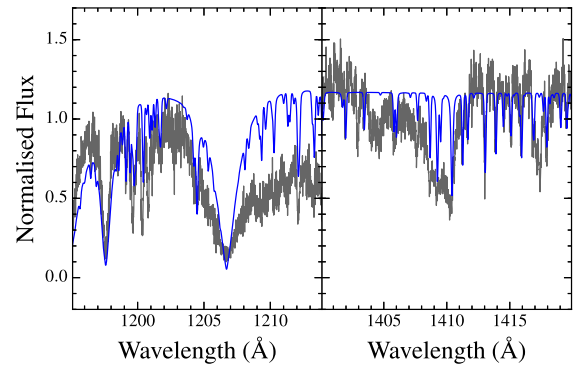


Figure 4. The model fit to the FUV spectrum underpredicts the red wing of the 1206 Å Si III resonance line and what appear to be Si lines around 1400 Å. The reason for the poor fit in these areas is unknown, but a similar feature is seen in GALEX 1931+0117 (see fig. 4 in Gänsicke et al. 2012).

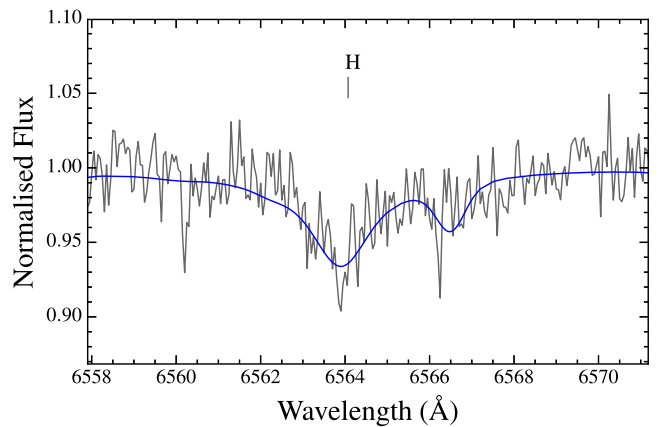


Figure 5. Section of our UVES spectrum showing a weak $\text{H}\alpha$ absorption line. Fitting an atmospheric model (blue) to the spectrum results in $\log(\text{H}/\text{He}) = -5.10 \pm 0.50$.

(2009) and Catalán et al. (2008), we find a progenitor mass of $\sim 2.7 M_{\odot}$, similar to most metal-polluted white dwarfs (Jura & Xu 2012; Koester et al. 2014a) and equivalent to an A-type star progenitor.

4 ACCRETION OF PLANETARY MATERIAL

The ultraviolet and optical spectra (Figs 1, 2 and 3) of SDSS J0845+2257 show metal absorption lines from a variety of elements (Figs 6 and 7), from which we can confidently measure the atmospheric abundances for hydrogen and 10 metals and place an upper limit on 4 further metals.

The spectra show many dozens to hundreds of lines of Mg, Si, Ca and Fe, so the measured abundances for those elements are fairly secure. The Ni abundance is confirmed by the clear and moderately strong lines at 1317 and 1370 Å. Our carbon abundance is based on more than 15 strong C I and C II lines between 1270 and 1470 Å and thus also fairly robust. The O abundance relies on the 7777, 7949 and 8448 Å lines shown in Fig. 6. As with Dufour et al. (2012), we find the abundance obtained using the 7949 Å absorption line to be highly discrepant with the other two lines. As the available atomic data for this line are limited, we have chosen to neglect this point, with the final abundance and error calculated from the remaining two lines. The 1152 and 1302 Å lines detected in the ultraviolet

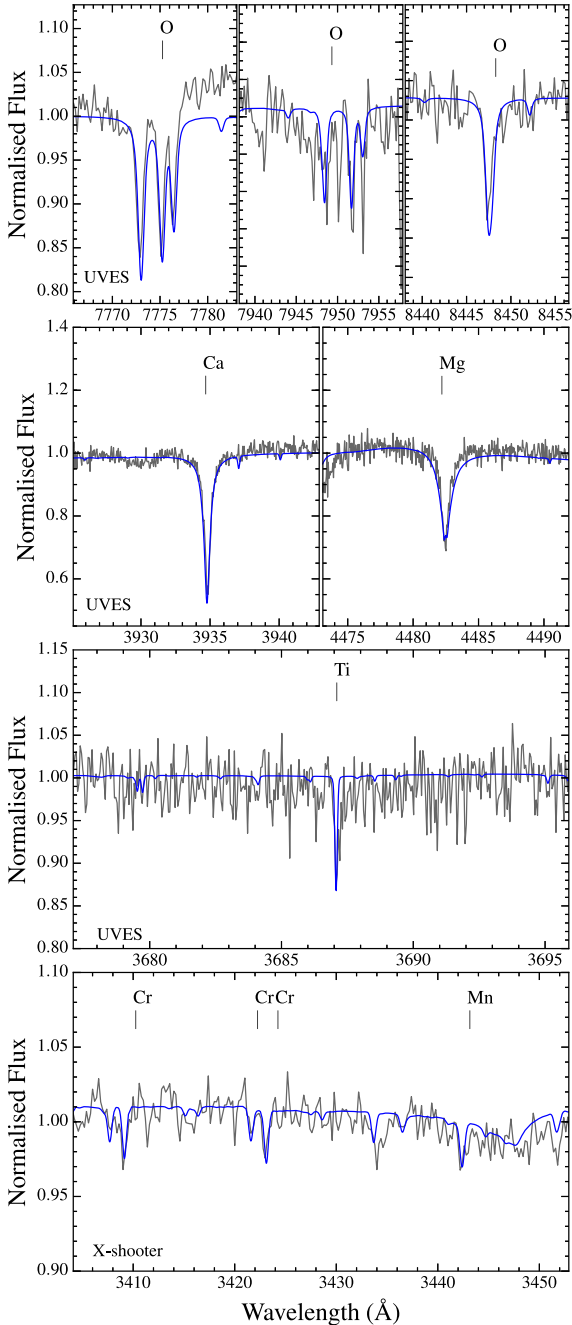


Figure 6. Normalized sections of X-Shooter and UVES spectra showing absorption lines from O, Ca, Mg, Ti, Cr and Mn, with the model atmosphere fit used to calculate the abundances overplotted in blue. The section shown in the top-middle panel is affected by telluric lines, which are not reproduced by our model.

spectra allow a less precise measurement which is compatible with this result.

One of the four metals for which we only present upper limits, Ti, is actually detected in our spectra. However, there is disagreement between the abundance measurements from lines at 3686 and 3762 Å, which fit the quoted abundance value, and the 3760 Å line, which is weaker than predicted by the model. Another line predicted by the model atmosphere, 3901 Å, is not observed. For these reasons, we only feel confident to present an upper limit for the abundance of Ti.

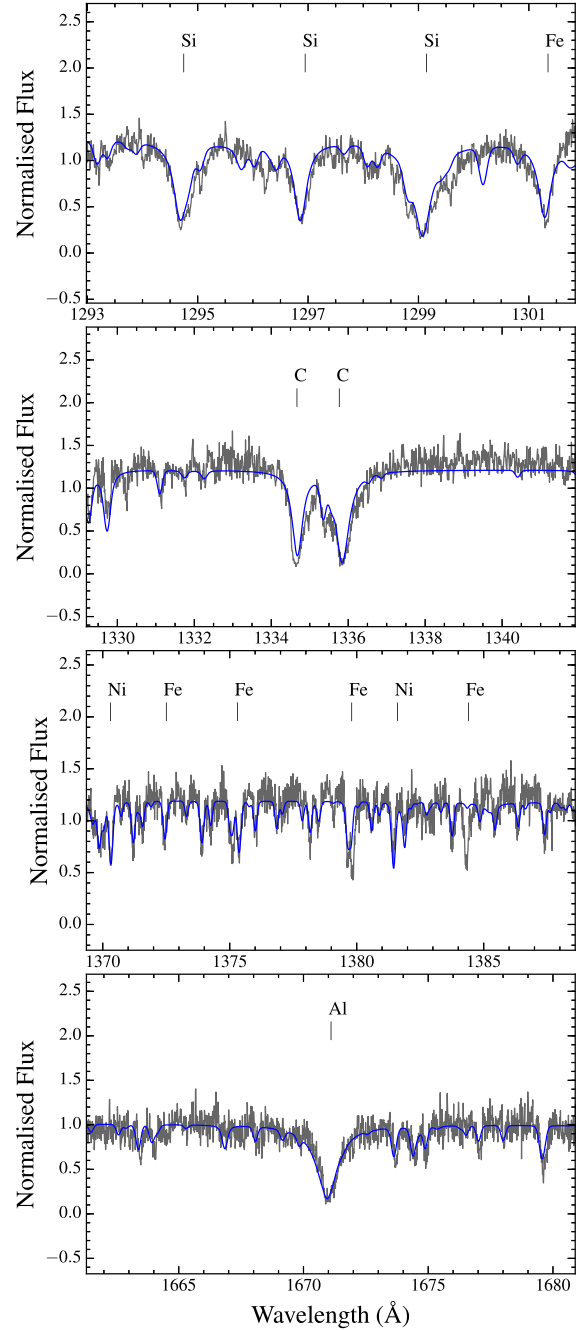


Figure 7. Sections of the COS FUV spectrum showing absorption lines from Si, C, Ni, Fe and Al, with the model atmosphere fit used to calculate the abundances overplotted in blue.

To study the composition of the progenitor object, we must compute the relative abundance ratios of the elements being accreted into the white dwarf atmosphere. These are not identical to the ratios of the photospheric metal abundances derived above, as individual metals sink out of the He envelope on different diffusion time-scales. The diffusion time-scales are a function of the depth of the convection zone and the diffusion velocity of each element, both of which vary with T_{eff} (Koester 2009).

SDSS J0845+2257 has a shallow ($\log(M_{\text{cvz}}/M_{\text{wd}}) = -8.4$) convection zone and we assume that the accreted metals are homogeneously mixed, such that the relative ratios of elements near the bottom of the convection zone are the same in the photosphere.

Table 2. Measured atmospheric abundances, computed diffusion time-scales and inferred metal accretion rates in the atmosphere of SDSS J0845+2257.

Element	$\log n(Z)/n(\text{He})$	$\tau_{\text{diff}}(10^4 \text{ yr})$	$\dot{M} (\text{g s}^{-1})$
1 H	-5.10 ± 0.50	n/a	n/a
6 C	-4.90 ± 0.20	1.5	4.1×10^8
7 N	≤ -6.30	1.5	$\leq 1.9 \times 10^7$
8 O	-4.25 ± 0.20	0.97	3.8×10^9
12 Mg	-4.70 ± 0.15	1.2	1.6×10^9
13 Al	-5.70 ± 0.15	1.2	1.9×10^8
14 Si	-4.80 ± 0.30	1.2	1.5×10^9
16 S	≤ -5.40	1.2	$\leq 4.3 \times 10^8$
20 Ca	-5.95 ± 0.10	0.97	1.9×10^8
21 Sc	≤ -7.70	0.65	$\leq 5.7 \times 10^6$
22 Ti	≤ -7.15	0.59	$\leq 2.4 \times 10^7$
24 Cr	-6.40 ± 0.30	0.53	1.6×10^8
25 Mn	-7.00 ± 0.40	0.49	4.6×10^7
26 Fe	-4.60 ± 0.20	0.87	6.6×10^9
28 Ni	-5.65 ± 0.30	0.44	1.2×10^9
Total			1.6×10^{10}

We calculate individual diffusion time-scales for each element (column 3 of Table 2) using the techniques described in Koester (2009),⁴ taking the total mass of helium in the convection zone to be $M(\text{He})_{\text{cvz}} = 2.605 \times 10^{-9} M_{\odot}$. The accretion rates of each element on to the white dwarf are then proportional to the ratio of the photospheric metal abundance to the diffusion time-scale, leading to the results in column 4 of Table 2.

The accretion/diffusion computations of Koester (2009) assume that accretion has been ongoing for $\gtrsim 5$ diffusion time-scales, reaching a steady state between material diffusing out of the convection zone and accreting on to the white dwarf. This assumption is likely valid as a dusty debris disc is detected (Brinkworth et al. 2012), which is almost certainly the source of the metals. Girven et al. (2012) showed that such discs have an estimated lifetime of several 10^5 yr. As the diffusion time-scales are only of the order of 10^4 yr, it is reasonable to assume that a steady state has been reached.

However, we cannot exclude the possibilities that the debris disc formed recently and that accretion and diffusion have not reached a steady state (the early phase), or that the accretion rate may not be constant over sufficiently long time-scales. The presence of a gaseous component to the debris disc (Section 5) has been suggested to be the result of dynamical activity in the disc (Veras et al. 2014a), which may affect the accretion rate. As the lifetime of the gaseous component is likely to be short relative to the diffusion time-scale (Wilson et al. 2014), its presence may be a sign of recent changes in the accretion rate. In this case, known as the instantaneous assumption, the relative chemical abundances in the accreted material will match the photospheric abundances. Jura et al. (2015) based their analysis of the debris composition on the instantaneous assumption, as at the $T_{\text{eff}} = 18700$ K used in their analysis the diffusion time-scales are much longer, making it much less likely for the accretion to have reached a steady state.

Table 3 shows the relative mass fractions of the elements under both the steady-state and early-phase/instantaneous scenarios. We find that the choice of accretion scenario has only a small effect on the elemental mass fractions, with the possible exceptions of C and Ni. Our discussion below of the debris composition is based on the

Table 3. Mass fractions of the accreted debris in the convection zone of SDSS J0845+2257 and in the bulk Earth (Allègre et al. 2001). In the early-phase/instantaneous approximation, the mass fractions are calculated using the atmospheric abundances, whilst in steady state the inferred accretion rates are used. The differences between the two approximations are small for most elements.

Element	Percentage by mass		Bulk Earth
	SDSS J0845+2257 Early phase	Steady state	
6 C	4.0 ± 1.8	2.5 ± 1.2	0.17
8 O	23.8 ± 11.0	23.4 ± 10.8	32.4
12 Mg	12.7 ± 4.4	9.9 ± 3.4	15.8
13 Al	1.4 ± 0.5	1.2 ± 0.4	1.5
14 Si	11.8 ± 8.1	9.3 ± 6.4	17.1
20 Ca	1.2 ± 0.3	1.2 ± 0.3	1.62
24 Cr	0.55 ± 0.38	0.99 ± 0.68	0.42
25 Mn	0.15 ± 0.13	0.28 ± 0.26	0.14
26 Fe	37.3 ± 17.1	40.8 ± 18.8	28.8
28 Ni	3.4 ± 2.4	7.5 ± 5.2	1.69
Other	3.7	2.9	1.08

steady-state assumption, but we note where the differences between steady-state and early-phase accretion are significant.

4.1 Total accretion rate and mass of the parent body

At $1.6 \times 10^{10} \text{ g s}^{-1}$, SDSS J0845+2257 has one of the highest inferred accretion rates detected at a metal-polluted white dwarf, with the observed elements representing the bulk of those making up the Earth (Table 3). Any additional undetected elements make up only trace amounts, so we can therefore draw reliable conclusions about the bulk abundances of the accreted material.

The total mass of metals calculated to be in the convection zone is $4.9 \times 10^{21} \text{ g}$, setting a lower limit on the mass of the accreted object (or objects). Assuming a rock-like density of $\rho \approx 2\text{--}4 \text{ g cm}^{-3}$, the mass is equivalent to a spherical object with an $\sim 130\text{--}170$ km diameter. However, detection of circumstellar gas (Gänsicke et al. 2008) and dust (Brinkworth et al. 2012) implies that accretion is still ongoing. If a large proportion of the debris is still in the disc, and/or has already sunk out of the convection zone of the white dwarf, then the total mass of the progenitor object may have been significantly higher than that currently present in the convection zone.

4.2 Carbon

Fig. 8 shows that the mass fraction of carbon in the accreted material for nearly all of the most heavily polluted white dwarfs is $\lesssim 0.5$ per cent, regardless of temperature, for both hydrogen (DA) and helium (DB) atmospheres. However, two DB white dwarfs, PG 1225–079 (Xu et al. 2013) and SDSS J0845+2257, have much higher carbon abundances. In PG 1225–079, which has a carbon mass fraction of 1.9 per cent, Xu et al. (2013) found no exact match of any Solar system object and suggested that the accretion may have been caused by two or more objects with different compositions. Jura et al. (2015) found a carbon mass fraction of 15 per cent in SDSS J0845+2257, which, assuming that all of the carbon was accreted, is consistent with that of interplanetary dust particles (IDPs). As IDPs are too small to make up the high inferred accretion rate, Jura et al. (2015) suggested that the disrupted rocky body was a Kuiper-belt analogue which lost its water content during the

⁴ See updated values at <http://www1.astrophysik.uni-kiel.de/~koester/astrophysics/astrophysics.html>

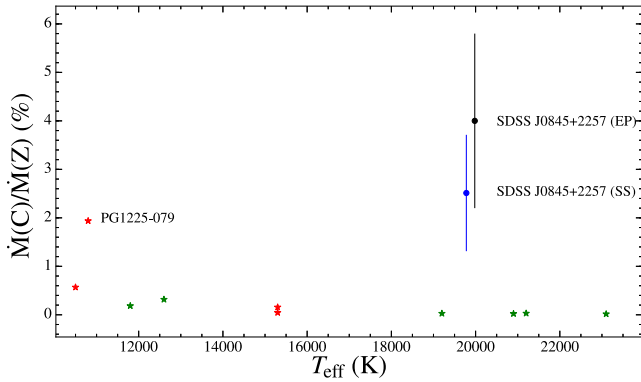


Figure 8. Mass fraction of carbon in the accreted material analysed in the most heavily polluted white dwarfs (Klein et al. 2011; Zuckerman et al. 2011; Dufour et al. 2012; Gänsicke et al. 2012; Farihi et al. 2013; Xu et al. 2013, 2014). Both the early-phase (black) and steady-state (blue) results for SDSS J0845+2257 are shown, with the marker for the early-phase offset by +200 K for clarity. Whilst the carbon fraction is low and roughly constant for both DA (green star symbols) and DB (red star symbols) white dwarfs regardless of T_{eff} , there are two clear outliers: PG 1225–079 (Xu et al. 2013) and SDSS J0845+2257.

post-main-sequence evolution of the system. Although our diffusion calculations still return an unusually high carbon abundance (2.5 per cent in steady state, 4.0 per cent in early phase), it is significantly lower than that found by Jura et al. (2015) and thus does not match the abundances found in IDPs. The large discrepancy between the carbon mass fractions derived from the two studies arises from the combination of a lower photospheric abundance of carbon determined from our COS ultraviolet spectroscopy (Section 3) and a systematically higher abundance of heavier elements. However, although the detailed results of the two studies differ, the fundamental conclusion of an unusually large abundance of carbon in the photosphere of SDSS J0845+2257, when compared to other debris-polluted white dwarfs, remains. We consider several alternative possible explanations for the excess carbon.

First, Veras, Shannon & Gänsicke (2014b) speculated that a small fraction of the debris at white dwarfs could be made up of ex-Oort cloud comets, which do have a substantial carbon fraction (Jessberger, Christoforidis & Kissel 1988). However, comets have a much higher water content than that observed here (Section 4.3) and cannot supply enough mass to explain the high rate and total amount of accreted metals.

Another scenario that could explain the high carbon abundance in SDSS J0845+2257 is based on results from terrestrial seismology, which have shown that a portion of the Earth’s core must be made up of less dense material than the majority Fe and Ni (Allègre et al. 1995). Carbon has been suggested as a possible candidate for this material (Poirier 1994; Zhang & Yin 2012). The enhanced levels of known core elements (Table 3, Section 4.5) at SDSS J0845+2257 could therefore explain the increased carbon abundance. However, the similarly enhanced level of core material detected in PG 0843+516 (Gänsicke et al. 2012) was not accompanied by an increase in the carbon mass fraction.

An alternative explanation is that the carbon present in the atmosphere of SDSS J0845+2257 has not been accreted from planetary debris, but is instead primordial to the white dwarf. A number of DB white dwarfs have been observed with atmospheric pollution from carbon, but no other metals (Provencal et al. 2000; Koester, Provencal & Gänsicke 2014b). These white dwarfs span a range of T_{eff} and no single explanation (in the absence of accretion)

can currently explain the high carbon abundances. At temperatures $\lesssim 16\,000$ K, convection can dredge up carbon from the core into the helium layer (Koester, Weidemann & Zeidler 1982), although some DBs have been observed with carbon abundances much lower than that predicted by this model (Desharnais et al. 2008). We note that the maximum contamination by dredge-up is thought to occur near 12 000 K (Pelletier et al. 1986), providing an entirely plausible source for the carbon detected in PG 1225–079 ($T_{\text{eff}} = 10\,800$ K; Xu et al. 2013). The carbon in hotter ($>20\,000$ K) white dwarfs, which cannot be explained by the classical dredge-up model, has been postulated to be raised by a weak stellar wind (Fontaine & Brassard 2005), but there is currently no working model for the necessary wind acceleration. Both the dredge-up and stellar wind models predict a very low carbon abundance in the temperature range $\sim 17\,000$ – $20\,000$ K.

However, the efficiency of photospheric carbon pollution by dredge-up depends not only on the depth of the convection zone, but also on the total mass of the helium layer (Weidemann & Koester 1995). The bulk of the DQ white dwarfs can be modelled with helium envelopes of $\approx 10^{-3}$ – $10^{-2} M_{\odot}$ (e.g. Fontaine & Brassard 2005), which is in agreement with the helium masses predicted by stellar evolution models (e.g. Lawlor & MacDonald 2006). However, a number of DB white dwarfs (Koester et al. 2014b), cooler DQ (Dufour, Bergeron & Fontaine 2005; Koester & Knist 2006), as well as the recently discovered hot DQ white dwarfs (Dufour et al. 2007, 2008) have higher carbon abundances than predicted by the canonical dredge-up scenario, which can be explained with thinner helium layers (Althaus et al. 2009; Koester et al. 2014b). Assuming that the unusually high carbon abundances in SDSS J0845+2257 are a result of dredge-up would require a thin ($\log(M_{\text{He}}/M_{\text{wd}}) \sim -4.6$) helium layer. In the light of the ongoing discussion of carbon abundances in helium atmosphere white dwarfs, and in the absence of a robust sample of helium layer measurements for white dwarfs, we conclude that dredge-up is a plausible origin of the photospheric carbon in SDSS J0845+2257.

An independent evaluation of the origin of the atmospheric carbon may be provided by the models of Hartmann et al. (2014), which predict that even a relatively small mass fraction of carbon ($>10^{-4}$) in the circumstellar debris should lead to emission from gaseous C II at 8683 and 8697 Å. Given that we do detect emission from gaseous Ca II (Section 5), the non-detection of C II could be further evidence that the carbon is primordial to the white dwarf. Hartmann et al. (2011) applied the same model to the gaseous disc around SDSS J1228+1040, again finding that the absence of C II 8683 and 8697 Å emission features in spectra obtained by Gänsicke et al. (2006) requires a low ($\lesssim 0.5$ per cent) carbon mass fraction in the gas. Gänsicke et al. (2012) showed that SDSS J1228+1040 has an extremely low photospheric carbon abundance, unambiguously demonstrating that the debris disc in this system is indeed strongly carbon depleted.

4.3 Oxygen

Measurements of the oxygen abundance in the accreting white dwarf GD 61 by Farihi et al. (2013) suggested that a large fraction of the debris was made of water. To estimate the water content in the debris around SDSS J0845+2257, we follow the procedure of Farihi et al. (2013), assessing first oxygen carriers other than water. We assume that all of the accreting Mg, Al, Si and Ca is bound into MgO, Al₂O₃, SiO₂ and CaO. If the debris is a fragment of a differentiated object, then the Fe and Ni content may be split into oxides from the mantle and metallic Fe and Ni from the core, so we present three

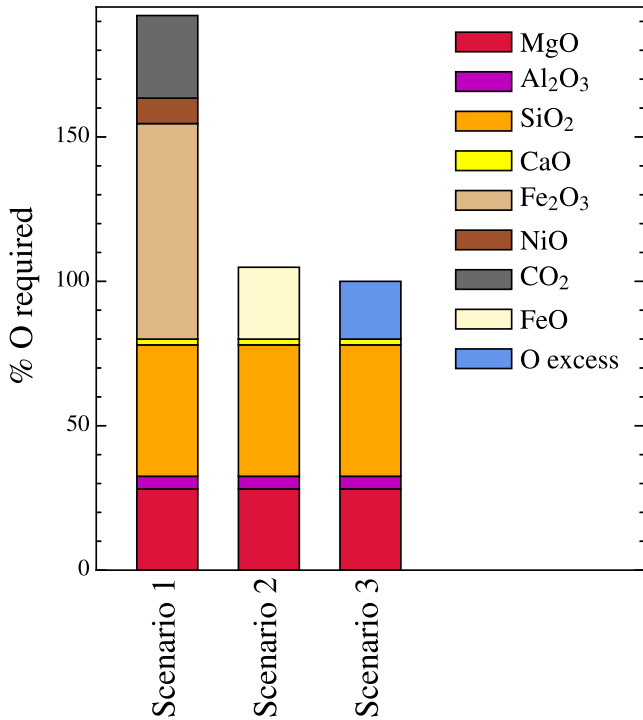


Figure 9. Oxygen budgets of the debris at SDSS J0845+2257, with three scenarios for different contributions of oxygen carriers: (1) all Fe as Fe_2O_3 , CO_2 and NiO present; (2) 50 per cent of Fe as FeO; (3) all Fe is metallic, making no contribution to the O budget. The third model is the only one to produce a marginal oxygen excess, suggesting that very little water was present in the parent body.

scenarios for the remaining elements (Fig. 9): (1) a conservative scenario where all of the Fe is bound into Fe_2O_3 , Ni into NiO and C into CO_2 ; (2) an intermediate scenario where C is primordial (see Section 4.2), the contribution from Ni is negligible and half the Fe is present as FeO; (3) a mantle-depleted scenario, discussed

further in Section 4.5, where there is no contribution from Fe, Ni or C. Only the third of these scenarios produces an oxygen excess, indicating that the accreted material was likely very dry regardless of the relative contributions from mantle and core material, as well as from carbon. This result is consistent with the low H abundance detected in the atmosphere (Table 2), and is not significantly altered under the assumption of early-phase or instantaneous accretion. Scenario 1 shows that there is insufficient oxygen to account for all of the potential carriers, an indicator that a large fraction of the Fe in the progenitor object was indeed metallic.

4.4 Refractory lithophiles

Fig. 10 compares the abundance of Ca and Al with respect to Si. These elements are two of the main refractory lithophiles: elements which sublime only at very high temperatures and are therefore found mainly in the mantle and crust of differentiated objects (Grossman 1972). The ratio of these two elements is nearly constant in most Solar system bodies, such that there is a linear correlation between Ca/Si and Al/Si. The Ca and Al accreting on to SDSS J0845+2257, as well as on to the other heavily polluted white dwarfs, also falls on to or near this line. This indicates that similar geochemical processes are taking place in these systems, and strengthens the case that analysing the accreted debris in the white dwarf photosphere provides a reliable representation of the chemical composition of a terrestrial object at SDSS J0845+2257.

4.5 Iron and nickel

Table 3 shows that the dominant element in the debris at SDSS J0845+2257 is Fe, with a mass fraction of 40.8 per cent, substantially higher than that in the Earth. Ni, which is the other major component in the Earth's core (McDonough 2000), is also enhanced relative to the Earth. Fig. 10 shows the linear relationship between Fe/Si and Ni/Si found in the Solar system bodies. Whilst the heavily polluted DB white dwarfs also fall on this line, the DA white dwarfs are less confined. SDSS J0845+2257 is close to the

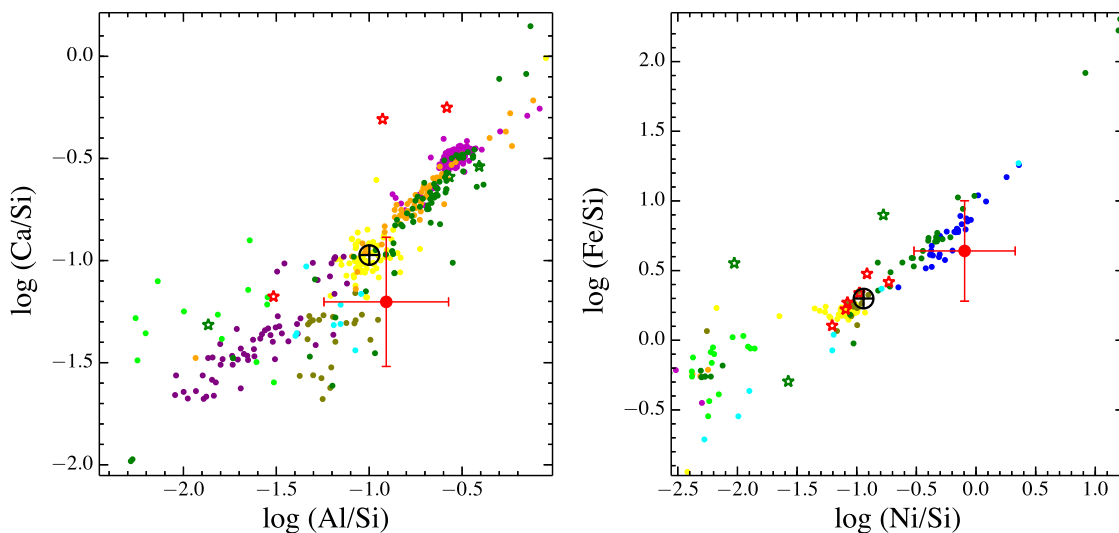


Figure 10. Comparison of the abundance of Al and Ca (left) and Fe and Ni (right) in SDSS J0845+2257 (red marker) with the bulk Earth (\oplus) (McDonough 2000) and the allasite (blue), mesosiderite (dark green), IAB (cyan), urelite (light green), ordinary chondrite and carbonaceous chondrite (yellow), enstatite chondrite (green-brown), howardite (orange), eucrite (magenta) and diogenite (purple) meteorites (Nittler et al. 2004). The most heavily metal-polluted white dwarfs are plotted as green (DAZ) and red (DBZ) stars (Klein et al. 2011; Zuckerman et al. 2011; Dufour et al. 2012; Gänsicke et al. 2012; Farihi et al. 2013; Xu et al. 2013, 2014). All abundances are normalized to Si.

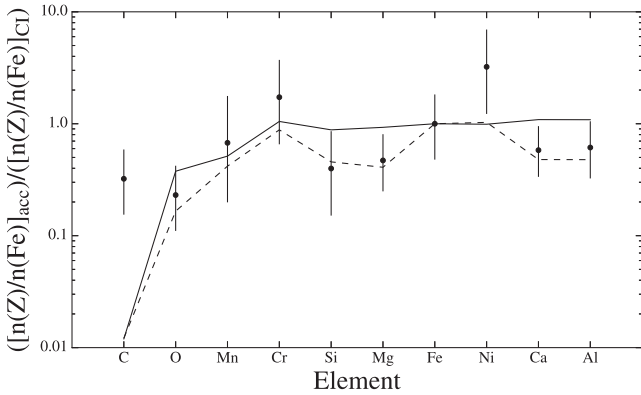


Figure 11. Elemental abundances of the accretion on to SDSS J0845+2257 relative to the abundance in CI chondrites, both normalized to Fe (black dots). The condensation temperature of the elements increases to the right. The solid line shows the abundances of the bulk Earth, whilst the dotted line shows a ‘wind-stripped’ model (Melis et al. 2011) in which approximately 15 per cent of the silicate Earth has been removed.

trend but has a higher Ni/Fe ratio (≈ 0.2) than the Earth (0.06). In the early-phase model, the Ni/Fe ratio drops to ≈ 0.09 .

The high Fe and Ni abundances suggest that the progenitor of the debris at SDSS J0845+2257 may have been a fragment of a larger, differentiated planetesimal with a relatively large core. This could be evidence that some of the processes thought to be responsible for Mercury’s large core, such as partial volatilization (Cameron 1985) or iron/silicate fractionation (Weidenschilling 1978), also occur in extrasolar planetary systems. However, it is likely that any planet close enough to its star for these processes to occur would have been engulfed during the red giant phase, unless it migrated outwards after formation.

Melis et al. (2011) proposed an alternative model in which a planetesimal is eroded by the intense stellar wind during the asymptotic giant branch (AGB). Fig. 11 shows this model applied to SDSS J0845+2257. Following the technique detailed in Melis et al. (2011), we show the abundances of the material accreted on to the white dwarf (Table 2) relative to the abundances in the CI chondrites (Lodders 2003), both of which are normalized to Fe. Combining the abundances for the core and silicate Earth from McDonough (2000), we normalize the abundances in the bulk Earth in the same way (solid black line). We then remove ~ 15 per cent of the silicate material (dotted line in Fig. 11), simulating the erosion of the mantle of a terrestrial object by stellar wind. We neglect any contribution from the crust, as it makes up only ≈ 0.5 per cent of the silicate Earth (Allègre et al. 1995). As can be seen in Fig. 11, the dominant elements of both Earth and SDSS J0845+2257 (e.g. Si, O, Mg, Ca, Al) appear to support this model, whilst the trace elements (Mn, Cr) are consistent with both scenarios. The high abundances of C (if accreted, see Section 4.2) and Ni remain unexplained, although Ni does become consistent with the model under the early-phase assumption. We note that, whilst Jura (2008) explored the effects of stellar winds on small asteroids, no detailed modelling has been done for the stripping of larger objects and it is unclear if the stellar wind during the AGB can provide the level of erosion suggested here and in Melis et al. (2011).

5 VARIABILITY OF THE CA II TRIPLET

SDSS J0845+2257 is part of a rare subset of metal-polluted white dwarfs that show double-peaked emission in the 8600 Å Ca II triplet,

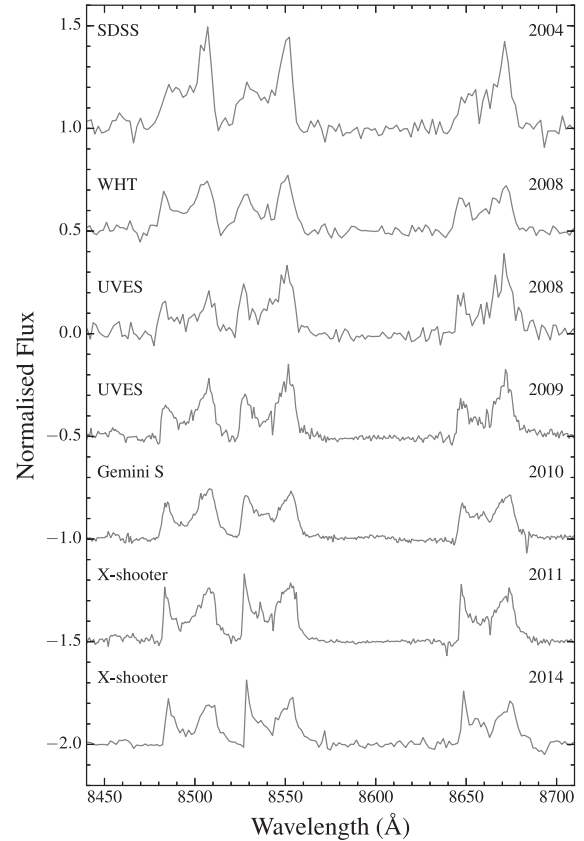


Figure 12. Time series spectra of the Ca II 8600 Å emission line triplet, plotted on the same scale with each successive spectrum offset by -0.5 . The SDSS data from 2004 show a pronounced asymmetry between the two peaks, with the red peak significantly greater in strength. This difference has since vanished, although in the most recent two spectra the blue peak appears marginally stronger.

indicative of a gaseous component to the debris disc (Gänsicke et al. 2006, 2008; Gänsicke, Marsh & Southworth 2007; Gänsicke 2011; Farihi et al. 2012; Melis et al. 2012; Wilson et al. 2014). The formation and evolution of these gaseous discs is still poorly understood, as the gas resides outside of the sublimation radius, within which gas is naturally expected to be present, and they are found at only a small fraction of the white dwarfs with dusty discs. There is no known case of a purely gaseous disc.

Time series observations of the 8600 Å Ca II triplet are shown in Fig. 12. The double-peaked morphology arises from the Doppler shifts induced by the Keplerian velocity of the material in the disc (Horne & Marsh 1986), a consequence of which is that the inner and outer radii of the disc can be estimated from the total width and peak separation of the Ca II lines, respectively. We find $R_{\text{in}} \sin^2 i \approx 0.3 R_{\odot}$ and $R_{\text{out}} \sin^2 i \approx 0.8 R_{\odot}$ (where i is the unknown inclination of the disc), consistent with the measurements of Gänsicke et al. (2008). Modelling the observed infrared excess, Brinkworth et al. (2012) estimated the extent of the dusty disc to extend from $R_{\text{in}} \approx 0.17 R_{\odot}$ to $R_{\text{out}} \approx 99.7 R_{\odot}$, although the outer radius of the disc is unconstrained due to the lack of observations at longer wavelengths. The overlap of these values strongly suggests that the gaseous and dusty components are co-orbital. Hartmann et al. (2014) attempted to better constrain the parameters of the gaseous disc component using a non-local thermodynamic

Table 4. Change in the equivalent width of the Ca II 8600 Å emission line triplet. The strength of the triplet dropped in the period 2004–2008, but has remained stable to within 1σ since.

Date	Ca II 8600 Å equivalent width (Å)
2004 December 19	-16.9 ± 2.2
2008 January 02	-10.3 ± 1.3
2008 April 03	-10.8 ± 1.4
2009 April 10	-11.4 ± 1.4
2010 April 02	-10.5 ± 1.3
2011 January 29	-12.8 ± 1.5
2014 October 20	-8.6 ± 1.1

equilibrium spectral model, but were unable to obtain a satisfactory fit to the emission lines.

The debris discs have provided some of the clearest evidence for variability in evolved planetary systems, in particular the rapid appearance and loss of the gaseous disc around SDSS J1617+1620 (Wilson et al. 2014) and the drop in infrared luminosity from the dust at WD J0959–0200 (Xu & Jura 2014). Similar, although less pronounced, changes are observed in the 8600 Å Ca II emission line triplet of SDSS J0845+2257. Table 4 lists the change in equivalent widths of the Ca II emission lines over time. The equivalent width was calculated over all three double-peaked lines to avoid systematic uncertainties caused by the overlap between the 8495 and 8542 Å components. The main source of uncertainty in the measurement is the polynomial fit used to normalize the spectrum. To account for this, the fit was varied slightly and the resulting scatter in the equivalent width measurements was incorporated into the stated error. The data demonstrate a $\approx 1/3$ drop in the equivalent width of the emission lines between 2004 and 2008, but the strength of the lines has remained constant to within 1σ since then. In addition, the time series spectra (Fig. 12) show pronounced changes in the morphology of the lines. In 2004 SDSS observations in the redshifted peaks were substantially stronger, but in more recent observations they have decreased in strength. Conversely, the blueshifted peaks have grown, to the extent that they have become slightly stronger than the red peaks in the latest observations. Due to the relatively low cadence of the time series observations compared with SDSS J1617+1620 (Wilson et al. 2014), we can only speculate about the cause of this variability, e.g. the interaction with a debris stream formed by a tidally disrupted planetesimal (see for example Debes, Walsh & Stark 2012; Veras et al. 2014a).

In addition to the Ca II emission line triplet, some of our spectra show double-peaked emission around the Fe II 5170 Å line (Fig. 13, left-hand panel). The Fe II emission is weaker and less variable than the emission from Ca II, with an average equivalent width of -0.8 ± 0.5 Å. Hartmann et al. (2011) predicted emission from the gaseous disc from 2797 Å Mg II, and detected it in the *HST* spectrum of SDSS J1228+1040. We do not detect emission from Mg II in SDSS J0845+2257 (Fig. 13), although the observed Mg II absorption line triplet is weaker than that predicted by the model atmosphere fit, possibly due to a small flux contribution from a disc emission line.

It is intriguing that the two white dwarfs with the highest and third highest inferred accretion rates, SDSS J0738+1835 (Dufour et al. 2012) and SDSS J0845+2257, respectively, both host debris discs with gaseous components. Unfortunately, measurements of the total metal accretion rate have only been made for five gas-hosting white

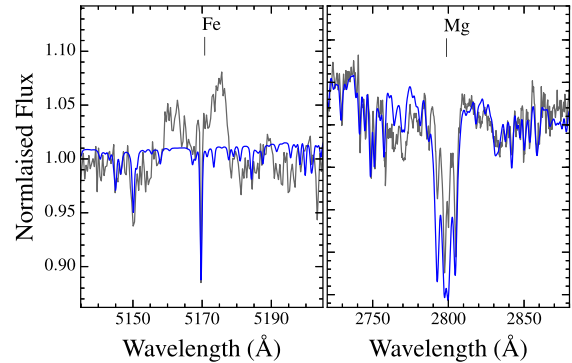


Figure 13. Left: example of weak double-peaked emission from Fe II. Right: the emission from Mg II predicted by Hartmann et al. (2014) is not detected, but could be masked by the photospheric absorption lines. The model atmosphere fit (blue) overpredicts the strength of the Mg II absorption, which could be due to some flux contribution by emission from the gaseous disc.

dwarfs to date,⁵ so the sample size is too small to reliably test any correlation between the presence of gas and the accretion rate.

6 SHORT-TERM VARIABILITY

We used the time-tag *HST*/COS photon event files to construct a light curve. To perform the background subtraction for each of the six individual G130M/G160M observations, we defined two regions on the COS detector, one below and one above the spectrum. The 1200 Å Ni I, 1216 Å Lyman α and 1302 Å O I airglow emission lines were masked and the edges of the detector segments excluded to reduce the instrumental noise. Fig. 14 shows a background-subtracted, normalized light curve binned to 5 s.

To probe for any variability in the flux from SDSS J0845+2257 caused by ongoing metal accretion, we used a χ^2 test, constructing a light curve using a bin size of 32 ms, i.e. the intrinsic time resolution of COS in time-tag mode. The box for the extraction of the spectrum was defined so that all counts of the target were included, while minimizing the amount of background contribution. We set our null hypothesis that each light-curve chunk is constant at the mean value. We find that a constant light curve has an 8–90 per cent probability of having the observed distribution, meaning that we cannot reject the hypothesis that the light curve is constant. The large range in probability is caused by the different total exposure times of the individual light-curve chunks.

To confirm this result and investigate any contribution to the variability from the background we repeated the process, this time with a wider box for extracting the spectrum to incorporate more background counts, as well as an identical test across the whole light curve. The difference in the results is not significant, so we conclude that the *HST*/COS data do not show significant variability on time-scales of 32 ms to ≈ 30 min.

As is obvious from Fig. 14, no transits by planets or planetesimals are detected. This non-detection is unsurprising, due to both the short duration of the observations and the fact that close-in planets around white dwarfs are probably rare (Veras & Gänsicke 2015).

⁵ SDSS J0738+1835 (Dufour et al. 2012), SDSS J1228+1040 (Gänsicke et al. 2012), He 1349-2305 (Melis et al. 2012), SDSS J1617+1620 (Wilson et al. 2014) and SDSS J0845+2257 (this work).

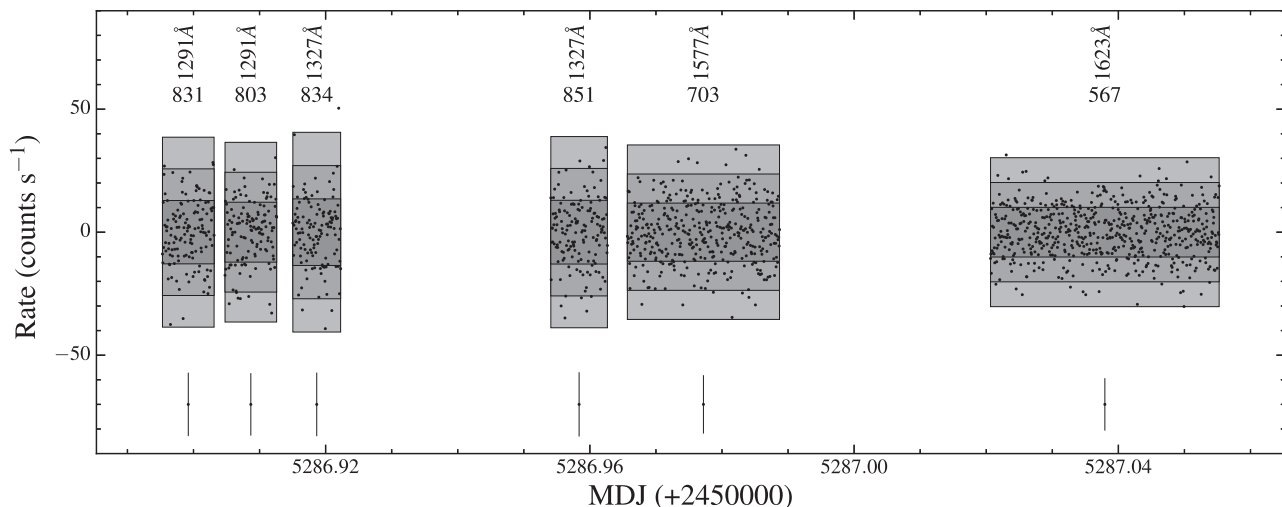


Figure 14. Background-subtracted, normalized light curves of SDSS J0845+2257, extracted from the *HST*/COS time-tag data. Dark grey, grey and light grey areas represent 1σ , 2σ and 3σ standard deviations from the mean, respectively, assuming a normal distribution for the count rate in each observation. The vertical and horizontal numbers above each spectrum are the central wavelength and mean count rate, respectively. An error bar showing the typical photon noise is shown beneath each spectrum.

7 CONCLUSION

We have carried out a detailed spectroscopic study, over a wide wavelength range, of the metal-polluted white dwarf SDSS J0845+2257. The star is accreting debris at a rate of $1.6 \times 10^{10} \text{ g s}^{-1}$ and the mass of metals in the convection zone implies a parent body $\gtrsim 100$ km in diameter. Measurements of 10 metals have shown that the disrupted planetesimal was similar to the Earth in composition, with a differentiated chemistry dominated by O, Mg, Si and Fe. The relatively high levels of Fe and Ni suggest that the planetesimal may have had a portion of its mantle stripped during the AGB phase, leaving a composition dominated by core material. An unusually large amount of carbon is present, although this could be primordial to the white dwarf. The white dwarf is also orbited by a debris disc with a mildly variable gaseous component.

ACKNOWLEDGEMENTS

The authors thank M. Jura and the referee, P. Dufour, for constructive discussions regarding the differences in our studies of this object, and C. Manser for performing the telluric correction to the X-shooter spectrum. The research leading to these results has received funding from the European Research Council under the European Union's Seventh Framework Programme (FP/2007-2013)/ERC Grant Agreement no. 320964 (WDTracer). SGP acknowledges financial support from FONDECYT in the form of grant number 3140585.

This paper is based on observations made with the NASA/ESA *Hubble Space Telescope*, obtained at the Space Telescope Science Institute, which is operated by the Association of Universities for Research in Astronomy, Inc., under NASA contract NAS 5-26555. These observations are associated with programme ID 11561.

This paper has also made use of observations from the SDSS-III, funding for which has been provided by the Alfred P. Sloan Foundation, the Participating Institutions, the National Science Foundation and the US Department of Energy Office of Science.

Observations were also made with the William Herschel Telescope on the island of La Palma by the Isaac Newton Group in the Spanish Observatorio del Roque de los Muchachos of the Instituto

de Astrofísica de Canarias, the Gemini South Telescope under programme GS-2010A-Q-17 and with the ESO VLT at the La Silla Paranal Observatory under programme IDs 081.C-0466(A), 082.C-0495(A), 383.C-0695(A), 386.C-0218(B) and 094.D-0344(A).

REFERENCES

- Aannestad P. A., Sion E. M., 1985, 90, 1832
 Allègre C. J., Poirier J., Humler E., Hofmann A. W., 1995, *Earth Planet. Sci. Lett.*, 134, 515
 Allègre C., Manhès G., Lewin E., 2001, *Earth Planet. Sci. Lett.*, 185, 49
 Althaus L. G., García-Berro E., Córscico A. H., Miller Bertolami M. M., Romero A. D., 2009, *ApJ*, 693, L23
 Barber S. D., Kilic M., Brown W. R., Gianninas A., 2014, *ApJ*, 786, 77
 Barstow M. A., Barstow J. K., Casewell S. L., Holberg J. B., Hubeny I., 2014, *MNRAS*, 440, 1607
 Bergeron P. et al., 2011, *ApJ*, 737, 28
 Brinkworth C. S., Gänsicke B. T., Girven J. M., Hoard D. W., Marsh T. R., Parsons S. G., Koester D., 2012, *ApJ*, 750, 86
 Cameron A. G. W., 1985, *Icarus*, 64, 285
 Casewell S. L., Dobbie P. D., Napiwotzki R., Burleigh M. R., Barstow M. A., Jameson R. F., 2009, *MNRAS*, 395, 1795
 Catalán S., Isern J., García-Berro E., Ribas I., 2008, *MNRAS*, 387, 1693
 Chayer P., 2014, *MNRAS*, 437, L95
 Chayer P., Fontaine G., Wesemael F., 1995, *ApJS*, 99, 189
 Chen Y.-P., Trager S. C., Peletier R. F., Lançon A., Vazdekis A., Prugniel P., Silva D. R., Gonneau A., 2014, *A&A*, 565, A117
 Debes J. H., Walsh K. J., Stark C., 2012, *ApJ*, 747, 148
 Dekker H., D'Odorico S., Kaufer A., Delabre B., Kotzłowski H., 2000, in Iye M., Moorwood A. F., eds, *Proc. SPIE Conf. Ser. Vol. 4008, Optical and IR Telescope Instrumentation and Detectors*. SPIE, Bellingham, p. 534
 Desharnais S., Wesemael F., Chayer P., Kruk J. W., Saffer R. A., 2008, *ApJ*, 672, 540
 Dufour P., Bergeron P., Fontaine G., 2005, *ApJ*, 627, 404
 Dufour P., Liebert J., Fontaine G., Behara N., 2007, *Nature*, 450, 522
 Dufour P., Fontaine G., Liebert J., Schmidt G. D., Behara N., 2008, *ApJ*, 683, 978
 Dufour P., Kilic M., Fontaine G., Bergeron P., Melis C., Bochanski J., 2012, *ApJ*, 749, 6
 Farihi J., Jura M., Zuckerman B., 2009, *ApJ*, 694, 805

- Farihi J., Gänsicke B. T., Steele P. R., Girven J., Burleigh M. R., Breedt E., Koester D., 2012, *MNRAS*, 421, 1635
- Farihi J., Gänsicke B. T., Koester D., 2013, *Science*, 342, 218
- Fontaine G., Brassard P., 2005, in Koester D., Moehler S., eds, *ASP Conf. Ser. Vol. 334, 14th European Workshop on White Dwarfs*. Astron. Soc. Pac., San Francisco, p. 49
- Gänsicke B. T., 2011, in Schuh S., Drechsel H., Heber U., eds, *AIP Conf. Ser. Vol. 1331, Planetary Systems Beyond the Main Sequence*. Am. Inst. Phys., New York, p. 211
- Gänsicke B. T., Marsh T. R., Southworth J., Rebassa-Mansergas A., 2006, *Science*, 314, 1908
- Gänsicke B. T., Marsh T. R., Southworth J., 2007, *MNRAS*, 380, L35
- Gänsicke B. T., Koester D., Marsh T. R., Rebassa-Mansergas A., Southworth J., 2008, *MNRAS*, 391, L103
- Gänsicke B. T., Koester D., Farihi J., Girven J., Parsons S. G., Breedt E., 2012, *MNRAS*, 424, 333
- Genest-Beaulieu C., Bergeron P., 2014, *ApJ*, 796, 128
- Gesicki K., Zijlstra A. A., Hajduk M., Szyszka C., 2014, *A&A*, 566, A48
- Girven J., Gänsicke B. T., Steeghs D., Koester D., 2011, *MNRAS*, 417, 1210
- Girven J., Brinkworth C. S., Farihi J., Gänsicke B. T., Hoard D. W., Marsh T. R., Koester D., 2012, *ApJ*, 749, 154
- Graham J. R., Matthews K., Neugebauer G., Soifer B. T., 1990, *ApJ*, 357, 216
- Green R. F., Schmidt M., Liebert J., 1986, *ApJS*, 61, 305
- Green J. C. et al., 2012, *ApJ*, 744, 60
- Grossman L., 1972, *Geochim. Cosmochim. Acta*, 36, 597
- Hartmann S., Nagel T., Rauch T., Werner K., 2011, *A&A*, 530, A7
- Hartmann S., Nagel T., Rauch T., Werner K., 2014, *A&A*, 571, A44
- Holberg J. B., Bergeron P., 2006, *AJ*, 132, 1221
- Hook I. M., Jørgensen I., Allington-Smith J. R., Davies R. L., Metcalfe N., Murowinski R. G., Crampton D., 2004, *PASP*, 116, 425
- Horne K., Marsh T. R., 1986, *MNRAS*, 218, 761
- Jessberger E. K., Christoforidis A., Kissel J., 1988, *Nature*, 332, 691
- Jura M., 2003, *ApJ*, 584, L91
- Jura M., 2006, *ApJ*, 653, 613
- Jura M., 2008, *AJ*, 135, 1785
- Jura M., Xu S., 2012, *AJ*, 143, 6
- Jura M., Young E. D., 2014, *Annu. Rev. Earth Planet. Sci.*, 42, 45
- Jura M., Xu S., Klein B., Koester D., Zuckerman B., 2012, *ApJ*, 750, 69
- Jura M., Dufour P., Xu S., Zuckerman B., Klein B., Young E. D., Melis C., 2015, *ApJ*, 799, 109
- Klein B., Jura M., Koester D., Zuckerman B., 2011, *ApJ*, 741, 64
- Koester D., 2009, *A&A*, 498, 517
- Koester D., Knist S., 2006, *A&A*, 454, 951
- Koester D., Weidemann V., Zeidler E.-M., 1982, *A&A*, 116, 147
- Koester D., Gänsicke B. T., Farihi J., 2014a, *A&A*, 566, A34
- Koester D., Provençal J., Gänsicke B. T., 2014b, 568, A118
- Kowalski P. M., Saumon D., 2006, *ApJ*, 651, L137
- Lawlor T. M., MacDonald J., 2006, *MNRAS*, 371, 263
- Lodders K., 2003, *ApJ*, 591, 1220
- McDonough W., 2000, in Teisseyre R., Majewski E., eds., *Earthquake Thermodynamics and Phase Transformations in the Earth's Interior*. Academic Press, San Diego, p. 5
- Melis C., Farihi J., Dufour P., Zuckerman B., Burgasser A. J., Bergeron P., Bochanski J., Simcoe R., 2011, *ApJ*, 732, 90
- Melis C. et al., 2012, *ApJ*, 751, L4
- Nittler L. R., McCoy T. J., Clark P. E., Murphy M. E., Trombka J. I., Jarosewich E., 2004, *Antarct. Meteorite Res.*, 17, 231
- Pelletier C., Fontaine G., Wesemael F., Michaud G., Wegner G., 1986, *ApJ*, 307, 242
- Poirier J.-P., 1994, *Phys. Earth Planet. Inter.*, 85, 319
- Provençal J. L., Shipman H. L., Thejll P., Vennes S., 2000, *ApJ*, 542, 1041
- Raddi R., Gänsicke B. T., Koester D., Farihi J., Hermes J. J., Scaringi S., Breedt E., Girven J., 2015, *MNRAS*, 450, 2083
- Rocchetto M., Farihi J., Gänsicke B. T., Bergfors C., 2015, *MNRAS*, 449, 574
- Saumon D., Chabrier G., van Horn H. M., 1995, 99, 713
- Schlafly E. F., Finkbeiner D. P., 2011, *ApJ*, 737, 103
- Sion E. M., Aannestad P. A., Kenyon S. J., 1988, *ApJ*, 330, L55
- Steele P. R., Burleigh M. R., Dobbie P. D., Jameson R. F., Barstow M. A., Satterthwaite R. P., 2011, *MNRAS*, 416, 2768
- Tremblay P.-E., Bergeron P., Gianninas A., 2011, *ApJ*, 730, 128
- van Maanen A., 1917, *PASP*, 29, 258
- Veras D., Gänsicke B. T., 2015, *MNRAS*, 447, 1049
- Veras D., Leinhardt Z. M., Bonsor A., Gänsicke B. T., 2014a, *MNRAS*, 445, 2244
- Veras D., Shannon A., Gänsicke B. T., 2014b, *MNRAS*, 445, 4175
- Vernet J. et al., 2011, *A&A*, 536, A105
- Weidemann V., 1960, *ApJ*, 131, 638
- Weidemann V., Koester D., 1995, *A&A*, 297, 216
- Weidenschilling S. J., 1978, *Icarus*, 35, 99
- Wilson D. J., Gänsicke B. T., Koester D., Raddi R., Breedt E., Southworth J., Parsons S. G., 2014, *MNRAS*, 445, 1878
- Xu S., Jura M., 2014, *ApJ*, 792, L39
- Xu S., Jura M., Klein B., Koester D., Zuckerman B., 2013, *ApJ*, 766, 132
- Xu S., Jura M., Koester D., Klein B., Zuckerman B., 2014, *ApJ*, 783, 79
- Zhang Y., Yin Q.-Z., 2012, *Proc. Natl. Acad. Sci.*, 109, 19579
- Zuckerman B., 2015, 19th European White Dwarf Workshop, 493, 291
- Zuckerman B., Becklin E. E., 1987, *Nature*, 330, 138
- Zuckerman B., Koester D., Reid I. N., Hünsch M., 2003, *ApJ*, 596, 477
- Zuckerman B., Koester D., Melis C., Hansen B. M., Jura M., 2007, *ApJ*, 671, 872
- Zuckerman B., Melis C., Klein B., Koester D., Jura M., 2010, *ApJ*, 722, 725
- Zuckerman B., Koester D., Dufour P., Melis C., Klein B., Jura M., 2011, *ApJ*, 739, 101

This paper has been typeset from a $\text{\TeX}/\text{\LaTeX}$ file prepared by the author.